Available online at www.sciencedirect.com

ScienceDirect

journal homepage: http://www.elsevier.com/locate/euprot

Comparative proteomic analysis reveals characteristic molecular changes accompanying the transformation of nonmalignant to cancer lung cells

Daniela Cadinu[1,2], *Jagmohan Hooda*[1], *Md Maksudul Alam, Parimaladevi Balamurugan, Robert M. Henke, Li Zhang*[*]

Department of Molecular and Cell Biology, Center for Systems Biology, University of Texas at Dallas, 800 W. Campbell Road, Richardson, TX 75080, USA

ARTICLE INFO

Article history:
Received 29 October 2013
Received in revised form
24 December 2013
Accepted 14 January 2014
Available online 14 February 2014

Keywords:
iTRAQ
Proteomic
Lung cancer
Actin cytoskeleton
Protein network

ABSTRACT

To identify changes in proteins accompanying transformation of normal lung epithelial cells to cancer cells, we performed a comparative proteomic study using two cell lines representing matching normal and cancer cells. Strikingly, a good number of detected actin cytoskeletal proteins were preferentially downregulated in cancer cells, while similar numbers of proteins in other organelles were up or downregulated. We also found that the formation of stress fibers and focal adhesions were substantially decreased in cancer cells. Protein network analysis showed that the altered proteins are highly connected. These results provide novel insights into the molecular mechanism promoting lung cancer progression.

1. Introduction

Lung cancer is the leading cause of cancer-related mortality in the US and worldwide, and about 85% of the cases are non-small-cell lung cancer (NSCLC) [1,2]. Using established cancer cell lines has been very powerful in identifying molecular mechanisms underlying tumorigenesis. Notably, recent work has established a very useful pair of lung cell lines [3,4] that can be used to identify changes accompanying the transformation of molecular changes underlying the transformation of normal cells to malignant cells. They are the HBEC30KT and HCC4017 cell lines [3,4]. The HCC4017 cell line represents non-small-cell lung cancer (NSCLC) cells isolated from a cancer patient, while the HBEC30KT cell line represents the normal, nonmalignant bronchial epithelial cells developed from the same patient. Thus, this pair of cell lines provides a good model for identifying changes associated with cancer, not merely variations among different persons.

The advent of proteomic technologies has made it possible to systematically identify and characterize the alterations in proteins in cells undergoing various physiological and pathophysiological changes. Particularly, the isobaric tags for relative and absolute quantitation (iTRAQ) profiling technol-

[*] *Corresponding author*. Tel.: +1 972 883 5757; fax: +1 972 883 5759.
E-mail address: li.zhang@utdallas.edu (L. Zhang).
[1] These authors contributed to this work equally.
[2] Present address: Max-Planck-Institute for Neurological Research, c/o DESY, Notkestrasse 85, 22607 Hamburg, Germany.
2212-9685
http://dx.doi.org/10.1016/j.euprot.2014.01.001

ogy enables the quantitative and direct comparison of the levels of a large number of proteins in two or more samples [5,6]. The iTRAQ technology employs isobaric tags with the same total mass but different reporter group mass to label peptides, which are then detected by MS/MS mass spectrometry. iTRAQ can simultaneously identify and quantify the levels of over 1000 proteins in 2–8 samples [7]. iTRAQ provides a powerful method for identifying differentially expressed proteins [5]. Thus, we decided to apply the iTRAQ technology to identify the protein changes accompanying lung epithelial cells when they become malignant.

Using iTRAQ, we were able to consistently identify and detect the levels of over 1500 proteins in lung cells. Among them, the levels of over 100 proteins exhibited statistically significant differences in cancer cells, when compared to normal cells. Particularly, the levels of 36 proteins actively involved in the function of actin cytoskeleton and cell motility were selectively downregulated in cancer cells. Further GO analysis identified significant changes in the levels of a group of nuclear regulatory proteins in cancer cells. Network analysis suggested that certain regulatory proteins may play an important role in mediating the changes in proteins in other cellular compartments, such as those involved in actin cytoskeleton. These results show that proteomic analysis can identify important molecular changes underlying cancer cell progression.

2. Materials and methods

2.1. *Lung cell line maintenance and preparation of protein extracts*

HBEC30KT and HCC4017 cell lines representing normal and NSCLC cells [3,4] were provided by Dr. John Minna's lab (UTSW) as a gift. They were developed from the same patient and were maintained in ACL4 supplemented with 2% FBS under 5% CO_2 at 37 °C. 'HBEC30KT and HCC4017' cells were collected and lysed by using the RIPA buffer (Cell Signaling Technology) containing the protease inhibitor cocktail (Invitrogen) and phosphatase inhibitors. Protein concentrations were determined by using the BCA assay kit (Thermo Scientific).

2.2. *Protein isobaric labeling with iTRAQ reagents*

Proteins from HBEC30KT and HCC4017 cell lines were extracted, and protein concentration was detected, as described below for Western blotting analysis. Isobaric labeling was carried out as described [8] and according to the procedure recommended by the PennState Hershey College of Medicine Mass Spectrometry Core facility (http://med.psu.edu/web/core/proteinsmassspectometry/protocols/itraq). Briefly, 100 μg of proteins from each sample was reduced with 5 mM TCEP (tris-(2-carboxyethyl) phosphine) at 60 °C for 1 h. Cysteine residues were blocked with 18 mM iodoacetamide at room temperature for 30 min. Then, the proteins were precipitated with ice-cold acetone (90%, v/v) overnight at −20 °C and centrifuged. The protein pellets were washed with ice-cold 90% acetone and 20 mM TEAB (triethylammoniumbicarbonate) and air-dried. Protein pellets were then suspended in buffer containing 0.5 M TEAB–0.1% SDS, at a concentration of 5 mg/ml, and then digested with trypsin at 40 °C overnight. Isobaric labeling reagents were purchased from Applied Biosystems. 8plex isobaric labeling kit containing tags with a reporter mass ranging from 113 to 121 was used. Isobaric tagging iTRAQ reagent in isopropanol was added directly to the protein digest to reach a final concentration of 61% isopropanol. The mixture was incubated at room temperature for 2 h. The reaction was then quenched by addition of 100 μl of water. The eight labeled peptide pools were mixed together and lyophilized.

2.3. *Mass spectrometry*

The iTRAQ protein samples were analyzed by the PennState Hershey College of Medicine Mass Spectrometry Core facility. Prior to MS analysis, protein samples were fractionated and separated into 15 fractions by using 2D-LC. SCX Separations were performed on a passivated Waters 600E HPLC system, using a 4.6 mm × 250 mm PolySULFOETHYL Aspartamide column (PolyLC, Columbia, MD), at a flow rate of 1 ml/min. Buffer A contained 10 mM ammonium formate, pH 2.7, in 20% acetonitrile/80% water. Buffer B contained 666 mM ammonium formate, pH 2.7, in 20% acetonitrile/80% water. The gradient was Buffer A at 100% (0–22 min following sample injection), 0%→40% Buffer B (16–48 min), 40%→100% Buffer B (48–49 min), then isocratic 100% Buffer B (49–56 min), then at 56 min switched back to 100% Buffer A to re-equilibrate for the next injection. The first 26 ml of eluant (containing all flow-through fractions) was combined into one fraction, then 14 additional 2-ml fractions were collected. All 15 of these SCX fractions were dried down completely to reduce volume and to remove the volatile ammonium formate salts, then resuspended in 9 μl of 2% (v/v) acetonitrile, 0.1% (v/v) trifluoroacetic acid and filtered prior to reverse phase C18 nanoflow-LC separation. The fractionation was performed to purify the peptides and increase the sensitivity of MS. Information from all fractions were combined and analyzed as a whole in the end.

For 2nd dimension separation by reverse phase nanoflow LC, each SCX fraction was autoinjected onto a Chromolith CapRod column (150 mm × 0.1 mm, Merck) using a 5 μl injector loop on a Tempo LC MALDI Spotting system (ABI-MDS/Sciex). Buffer C was 2% acetonitrile, 0.1% trifluoroacetic acid, and Buffer D was 98% acetonitrile, 0.1% trifluoroacetic acid. The elution gradient was 95% C/5% D (2 μl/min flow rate from 0 to 3 min, then 2.5 μl/min from 3 to 8.1 min), 5% D→38% D (8.1–40 min), 38% D→80% D (41–44 min), 80% D→5% D (44–49 min) (initial conditions). Flow rate was 2.5 μl/min during the gradient, and an equal flow of MALDI matrix solution was added post-column (7 mg/ml recrystallized CHCA (a-cyano-hydroxycinnamic acid), 2 mg/ml ammonium phosphate, 0.1% trifluoroacetic acid, 80% acetonitrile).

After sample spot drying above, thirteen calibrant spots (ABI 4700 Mix) were added to each plate manually. MALDI target plates (15 per experiment) were analyzed in a data-dependent manner on an ABI 5800 MALDI TOF-TOFs. MS/MS spectra were taken by using up to 2500 laser shots per spectrum at Laser Power 3000, with CID gas Air at $1.2–1.3 \times 10^{-6}$ Torr. As each plate was entered into the instrument, a plate calibration/MS Default calibration update was

performed, and then the MS/MS default calibration was updated. MS spectra were then acquired from each sample spot using the newly updated default calibration, using 500 laser shots per spot, laser intensity 3200. A plate-wide interpretation was then automatically performed, choosing the highest peak of each observed *m/z* value for subsequent MS/MS analysis.

Up to 2500 laser shots at laser power 4200 were accumulated for each MS/MS spectrum. When the MS and MS/MS spectra from all 15 plates in a sample set had been acquired, protein identification and quantitation were performed using the Paragon algorithm as implemented in Protein Pilot 4.0 software, searching the spectra against either species-specific subsets (plus common contaminants) of the NCBInr database concatenated with a reversed "decoy" version of itself, or the entire NCBInr database. For ProteinPilot analyses, the preset Thorough Search settings were used, and identifications must have a ProteinPilot Unused Score > 1.3 (>95% Confidence interval) in order to be accepted. In addition, the only protein IDs accepted must have a "Local False Discovery Rate" estimation of no higher than 5%, as calculated from the slope of the accumulated Decoy database hits by the PSPEP (Proteomics System Performance Evaluation Pipeline) program by Sean Seymour and colleagues [9]. Note that this Local or "Instantaneous" FDR estimate is much more stringent than $p < 0.05$ or 95% confidence scores in Mascot, Sequest, ProteinPilot, or the aggregate False Discovery Rate estimations (2 × number of Decoy database IDs/Total IDs at any chosen threshold score) commonly used in the literature, and combined with the ProGroup algorithm included in ProteinPilot gives a very conservative and fully MIAPE-compliant list of proteins identified. The total human sequences searched contain 30345 Protein Sequences, plus 360 common lab contaminants. The Local False Discovery Rate (FDR) for the lowest ranking accepted protein ID was less than 5% with the *p*-value between <0.01 and <0.001.

2.4. Mass spectrometry data analysis

8plex iTRAQ MS/MS analysis was performed twice, with each set having 4 normal and 4 cancer cell samples. Therefore, we gained 4 sets of iTRAQ data for each experiment. From two experiments, we gained 8 sets of protein ratios comparing cancer cell line (HCC4017) with the normal cell line (HBEC30KT). Only those proteins that were identified in at least four experiments were considered as detected. Data from each experiment were normalized, and estimated changes in the relative amounts of each identified protein (i.e., cancer vs. normal cells) calculated. Each of the peptides identified from a specific protein is presented as a ratio, with a ratio of 1.0 representing no significant change. The mean and median ratios for each identified proteins were calculated in MS Excel. Proteins that showed ratios higher than 1 in all detected samples and had mean and median ratios of at least 1.3 were considered to be upregulated, while proteins that showed ratios less than 1 in all detected samples and had mean and median ratios of less than 0.76 were considered to be downregulated. The selected up- or downregulated proteins are listed in supplementary Tables S2 and S3. The statistical significance of altered proteins was further confirmed by using *p* values. The *p* values were calculated based on Fisher's method [10]. For all *p*-values p_i from *n* replicates, $x = -2 \times \sum[\ln(p_i)]$ was calculated, which follows *Chi-square* distribution with degree of freedom $2n$, to obtain the combinational *p*-value for one protein. Those with *p* values <0.05 are listed in Tables 2–5.

Gene Ontology (GO) analysis of identified proteins and up or downregulated proteins in cancer cells was performed by the NIH DAVID application. Protein interaction networks were constructed by using Pathway Studio version 7 and by using the GENEMANIA program.

2.5. Western blotting analysis

About 50 μg proteins from the cells were electrophoresed on 9% SDS-polyacrylamide gels, and then transferred onto the Immuno-Blot PVDF Membrane (Bio-Rad). The membranes were probed with the desired antibodies, followed by detection with a chemiluminescence Western blotting kit (Roche Diagnostics). The signals were detected by using a Carestream image station 4000MM Pro, and quantitation was performed by using the Carestream molecular imaging software version 5.0.5.30 (Carestream Health Inc.). Polyclonal anti-utrophin, anti-transgelin, and anti-NAMPT antibodies were purchased from Santa Cruz Biotechnology. Monoclonal anti-phospho-EphA2 (Ser897), anti-EphA2 and anti-β-actin antibodies were purchased from Cell Signaling Technology.

2.6. Immunofluorescence microscopy

For immunofluorescence microscopy, cells were grown on polylysine-coated slides and were fixed with 4% formaldehyde. Cells were washed two times with PBS containing 0.2% BSA and then permeabilized with 0.1% Triton X-100 containing 0.2% BSA. Immunofluorescence staining was performed as described [11]. Fluorescent images were acquired by using a multi-channel Zeiss Axio Observer.Z1 fluorescent microscope with a Zeiss 40× Oil immersion lens and with a high speed AxioCam MRm Rev3 monochrome camera. The software used was Carl Zeiss AxioVision Rel 4.8.1, set to the multi-dimensional mode that allows automatic filter changes and image capturing. Vinculin was stained with monoclonal anti-vinculin antibody (Sigma V9131). The secondary antibody used was FITC-conjugated goat anti-mouse antibody (Invitrogen A11017). F-actin was visualized with Alexa Fluor 568-phalloidin (Invitrogen A12380).

3. Results

3.1. iTRAQ detected over 1500 proteins in normal and lung cancer cells

We extracted proteins from both the normal, non-malignant bronchial epithelial cell line HBEC30KT and the NSCLC line HCC4017 [3,4]. We performed iTRAQ analysis of the proteins and obtained the ratios of proteins in cancer vs. normal cells in eight biological replicates (see Section 2 and supplementary Table S1). In total, we detected 1584 proteins with high statistical confidence (Table 1). The Local False Discovery Rate (FDR) for the lowest ranking accepted protein ID was less than 5% with the *p*-value between <0.01 and <0.001. The ratios from the

Table 1 – Summary of the proteins identified in HCC.

	Total	Nuc	Cyto-s	Cyto-p	Mito	ER	Act
Detected	1584	532	392	1182	241	192	118
Up	183 (53)	72 (17)	34 (14)	121 (38)	18 (5)	24 (8)	1 (1)
Down	275 (86)	52 (17)	51 (14)	204 (69)	34 (7)	19 (6)	81 (36)

The numbers shown here are the up or down regulated proteins selected by fold changes. The numbers in the parenthesis represent those with p value <0.05. Nuc, nucleus; Cyto-s, cytosol; Cyto-p, cytoplasm; Mito, mitochondria; ER, endoplasmic reticulum; Act, actin cytoskeleton.

eight biological replicates (see supplementary Table S1) were calculated and analyzed. The majority of the detected proteins were cytoplasmic, including 241 mitochondrial proteins and 118 cytoskeletal proteins (Table 1). 532 nuclear proteins were also detected. Evidently, iTRAQ provided the detection and comparison of the protein levels of a large number of proteins, which cannot be achieved by using other proteomic techniques, such as two-dimensional gel electrophoresis and mass spectrometry [12].

3.2. *iTRAQ data analysis shows that the levels of a number of detected proteins were consistently changed in lung cancer cells*

We combined eight sets of data from iTRAQ analysis (see supplementary Table S1) and identified proteins whose levels were consistently up- or downregulated in cancer cells using fold changes (see Section 2). Complete lists of up- or downregulated proteins and their ratios in cancer vs. normal cells are shown in supplementary Tables S2 and S3. Then, we calculated p values for the detected proteins (see Section 2 and supplementary Table S1). We further narrowed down upregulated and downregulated proteins by selecting only those with p values <0.05. Table 1 shows the data from both fold changes and those with p value cutoff. 183 proteins (53 with p values <0.05) were consistently upregulated by at least 1.3-fold, while 275 proteins (86 with p values <0.05) were consistently downregulated by at least 1.3-fold in cancer cells (with ratio of cancer vs. normal less than 0.76).

Furthermore, we decided to confirm the detected changes by using the conventional Western blotting (Fig. 1A–C). To avoid bias, we selected those with mean and median ranging from 3- to 6-fold randomly. Fig. 1 shows that the upregulated protein, nicotinamide phosphoribosyltransferase (NAMPT, see supplementary Table S2) was indeed upregulated (Fig. 1A), while the two downregulated proteins (see supplementary Table S3), transgelin (TAGLN, Fig. 1A) and utrophin (UTRN, Fig. 1B), were downregulated. The fold changes detected by Western blotting are largely consistent with the changes detected by iTRAQ. Ponceau staining showed that the total proteins loaded for normal and cancer cells were very similar; the variation was within 10% (data not shown). Furthermore, iTRAQ can detect only proteins with relatively high levels. Thus, many signaling proteins, such as cell surface receptor EphA2, which plays critical roles in cancer metastasis and is upregulated in about half of NSCLC tumor tissues [13,14], cannot be detected by iTRAQ. Compared to structural proteins, such as actin cytoskeletal proteins, signaling proteins are expressed at lower levels. However, by using Western blotting, we found that the Eph receptor, EphA2, was upregulated approximately 17-fold in cancer cells (Fig. 1C). The levels of

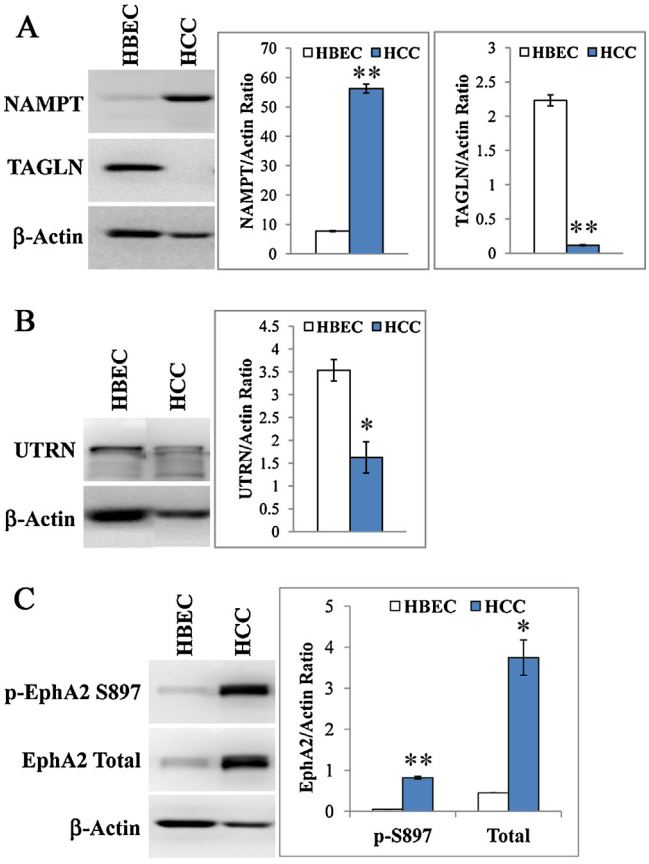

Fig. 1 – Western blotting analysis of selected proteins in normal and cancer lung cells. The normal HBEC30KT lung epithelial (HBEC) and NSCLC HCC4017 (HCC) cells were cultured, and proteins were extracted. Protein levels were detected by using Western blotting. (A) The levels of nicotinamide phosphoribosyltransferase (NAMPT) and transgelin (TAGLN) in normal and NSCLC cells. (B) The levels of utrophin (UTRN) in normal and NSCLC cells. (C) The levels of total and phosphorylated EphA2 receptor in normal and NSCLC cells. The protein level of β-actin in the samples was used for normalization. p values were calculated by using Welch 2-sample t-test. *, p value <0.05; **, p value <0.005.

both total and phosphorylated (ligand activated) EphA2 proteins were upregulated approximately 8-fold in cancer cells. This is consistent with previous studies showing that EphA2 is highly upregulated in metastatic cancers [15].

We performed Gene Ontology (GO) analysis to analyze the up- and downregulated proteins. Although applying p values substantially decreased the number of proteins changed

Table 2 – A list of actin cytoskeletal proteins downregulated in NSCLC cells.

Protein ID	Gene symbol	Description	Fold	*p*-Value
NP_001605	ACTG1	Actin, cytoplasmic 2	0.3	2.39E−03
NP_001005386	ACTR2	Actin-related protein 2	0.6	1.67E−02
NP_005712	ACTR3	Actin-related protein 3	0.3	3.18E−06
NP_653080	AKAP12	A-kinase anchor protein 12	0.4	7.45E−11
NP_001002858	ANXA2	Annexin A2 isoform 1	0.1	3.60E−68
NP_005709	ARPC4	Actin-related protein 2/3 complex subunit 4	0.5	4.10E−02
NP_004333	CALD1	Caldesmon isoform 2	0.1	7.12E−10
NP_001894	CTNNA1	Catenin alpha-1	0.4	1.67E−02
NP_060293	DUSP23	Dual specificity protein phosphatase 23	0.1	3.09E−03
NP_001104026	FLNA	Filamin-A isoform 2	0.2	4.46E−29
NP_001157791	FLNB	Filamin-B isoform 4	0.6	5.50E−03
NP_001157789	FLNB	Filamin-B isoform 1	0.5	4.33E−02
NP_001531	HSPB1	Heat shock protein beta-1	0.1	4.17E−09
NP_003861	IQGAP1	Ras GTPase-activating-like protein	0.5	1.54E−03
NP_000413	KRT17	Keratin, type I cytoskeletal 17	0.1	2.67E−05
NP_005547	KRT7	Keratin, type II cytoskeletal 7	0.3	3.22E−08
NP_002435	MSN	Moesin	0.6	1.36E−04
NP_001243024	MYH10	Myosin-10 isoform 3	0.1	1.12E−02
NP_002464	MYH9	Myosin-9	0.2	2.04E−55
NP_066299	MYL6	Myosin light polypeptide 6	0.4	1.06E−07
NP_006088	MYL9	Myosin regulatory light polypeptide 9	0.1	1.57E−02
NP_001074419	MYO1C	Myosin-Ic	0.2	1.84E−05
NP_006087	NDRG1	Protein NDRG1	0.1	4.40E−04
NP_976227	PDLIM7	PDZ and LIM domain protein 7	0.2	1.90E−04
NP_005013	PFN1	Profilin-1	0.6	2.04E−03
NP_004395	Sept2	Septin 2	0.6	2.98E−03
NP_003177	TAGLN	Transgelin	0.2	4.10E−03
NP_003555	TAGLN2	Transgelin-2	0.1	3.60E−16
NP_006280	TLN1	Talin-1	0.4	1.88E−11
NP_066932	TMSB4X	Thymosin beta-4	0.3	1.10E−02
NP_001018006	TPM1	Tropomyosin alpha-1 chain	0.6	2.79E−03
NP_705935	TPM3	Tropomyosin alpha-3 chain	0.7	2.22E−02
NP_001138632	TPM4	Tropomyosin alpha-4 chain	0.3	1.52E−06
NP_006073	TUBA1B	Tubulin alpha-1B chain	0.3	9.18E−09
NP_009055	UTRN	Utrophin	0.1	3.09E−02
NP_003452	ZYX	Zyxin	0.5	5.26E−03

in NSCLC cells, the trends of changes and the main conclusions remained remarkably unchanged (see Table 1 and data described below). For example, 124 (72 + 52; 17 + 17 with *p* value cutoff) out of 532 detected nuclear proteins were changed, while 52 (18 + 34; 5 + 7 with *p* value cutoff) out of 241 detected mitochondrial proteins were changed. The sensitivity of iTRAQ, not experimental artifacts, is likely responsible for the lower number of proteins with statistically significant *p* values. Thus, many detected changes may be valid, even though the *p* values are too high. The most striking change is that many (82 or 37 out of 118) of the detected proteins with functions in the formation and regulation of actin cytoskeleton were changed. Furthermore, among those actin cytoskeletal proteins changed in cancer cells, all but one of these proteins were downregulated in cancer cells (see column "Act" Table 1).

3.3. *Network analysis reveals characteristic changes underlying the transformation of lung cancer cells*

The most prominent change in lung cancer cells identified by iTRAQ and GO analysis is the downregulation of an overwhelming majority of detected proteins involved in the function and regulation of the actin cytoskeleton (see Tables 1 and 2). These proteins (Table 2) play important roles in the formation of actin stress fibers and in cell adhesion and motility [16–19]. These proteins form a complex network (Fig. 2) connecting the functions of actin cytoskeleton, adhesion and extracellular matrix. (For complete information and for comparison, changed proteins selected only by fold changes and those by both fold changes and *p* values are highlighted differently in the networks.) The downregulation of these proteins likely leads to the changes in actin cytoskeleton, cell–cell adhesion and cell motility accompanying cancer cell transformation.

Another important class of proteins that were changed in cancer cells are the nuclear proteins. We found that 72 (17 with *p* value cutoff) nuclear proteins were upregulated (Table 3), while 52 (17 with *p* value cutoff) were downregulated in cancer cells (Table 4). These nuclear proteins can interact with each other, and they form a very interconnected network (see Fig. 3). The result suggests that the coordinated changes in this network of nuclear proteins may lead to further downstream changes underlying cancer cell transformation. Indeed, many of these nuclear proteins have regulatory functions, and can affect proteins in other cellular compartments. For example, Fig. 4 shows that many of the changed nuclear proteins are directly connected to those changed proteins in actin cytoskeleton. Very likely, the changes in these nuclear proteins contribute, at least in part, to the changes in these

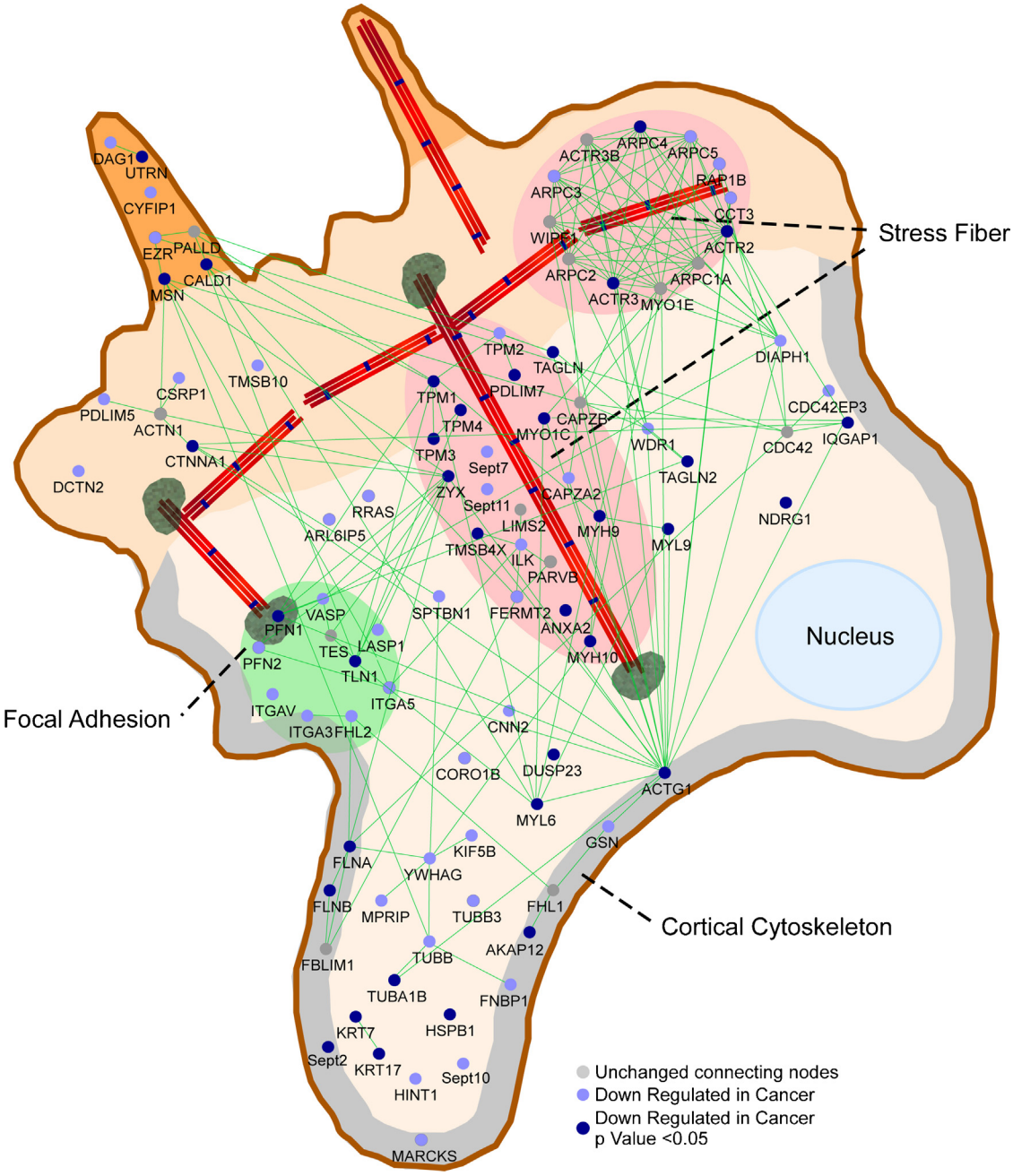

Fig. 2 – Graphical representation of protein-protein interaction networks for downregulated actin cytoskeletal proteins. The network was constructed using the tools and edge data available on the Genemania website. Node attribute assignment (GO terms and Expression) was performed in Cytoscape along with network arrangement. Final visuals were performed in CANVAS. Blue and light blue nodes represent proteins that are down regulated in cancer. Dark blue ones are selected based on both fold changes and *p* values, while light blue ones are selected based only on fold changes. Gray nodes represent unchanged proteins present in the network. Where possible nodes are positioned into sub-cellular features based on Gene Ontology terms. Lines represent an association of the protein to an interaction, a particular complex or functional GO term. The proteins shown in light red ovals are those involved in the formation of dorsal and ventral stress fibers. Proteins shown in the light green circle are those involved in focal adhesions. (For interpretation of the references to color in this figure legend, the reader is referred to the web version of the article.)

actin cytoskeletal proteins. For example, the changes in NCL (nucleolin) and PPP1CB may contribute to changes in the expression of actin cytoskeletal proteins, such as MYH9 and MYL9 (see Fig. 4).

Compared to nuclear proteins, the number of changed mitochondrial proteins is small (Table 1). Nonetheless, it is interesting to note that two proteins relating to heme synthesis and function [20], UQCRB and cytochrome c1 (Table 5),

Table 3 – A list of nuclear proteins upregulated in NSCLC cells.

Protein ID	Gene symbol	Description	Fold	*p*-Value
NP_001632	APEX1	D-(apurinic or apyrimidinic site) lyase	2.6	7.38E−05
NP_005785	DHRS2	Dehydrogese/reductase SDR family member 2	3.2	2.23E−05
NP_002005	FKBP4	Peptidyl-prolyl *cis–trans* isomerase FKBP4	2.2	1.90E−03
NP_005508	HMGN2	Non-histone chromosomal protein HMG-17	3.5	4.27E−02
NP_006382	IPO7	Importin-7	3	2.40E−06
NP_573566	LRPPRC	Leucine-rich PPR motif-containing protein	3.9	4.71E−14
NP_004528	NAP1L1	Nucleosome assembly protein 1-like 1	4.2	6.31E−03
NP_055680	NCAPD2	Non-SMC condensin I complex, subunit D2	87.9	8.12E−05
NP_005372	NCL	Nucleolin	2.8	1.81E−13
NP_001018146	NME1-NME2	NME1–NME2 protein	3.3	3.76E−11
NP_002559	PABPC1	Polyadenylate-binding protein 1	1.7	4.22E−03
NP_066953	PPIA	Peptidyl-prolyl *cis–trans* isomerase A	1.8	1.40E−02
NP_006436	PRPF8	Pre-mR-processing-splicing factor 8	9.7	2.20E−02
NP_116559	RECQL	ATP-dependent D helicase Q1	1.9	1.43E−02
NP_006704	SUB1	Activated RNAPII transcriptional coactivator p15	4.3	6.43E−09
NP_001153147	SYNCRIP	Heterogeneous nuclear ribonucleoprotein Q	1.9	4.44E−04
NP_001460	XRCC6	X-ray repair cross-complementing protein 6	1.5	3.58E−03

Table 4 – A list of nuclear proteins downregulated in NSCLC cells.

Protein ID	Gene symbol	Description	Fold	*p*-Value
NP_001611	AHNAK	Neuroblast differentiation-associated protein AHK	0.3	1.79E−39
NP_612429	AHNAK2	Protein AHNAK2	0.2	4.41E−02
NP_653080	AKAP12	A-kinase anchor protein 12	0.4	7.45E−11
NP_060293	DUSP23	Dual specificity protein phosphatase 23	0.1	3.09E−03
NP_001387	DYRK1A	Dual specificity tyrosine-phosphorylation-regulated kinase 1A	0.2	4.33E−02
NP_055416	EHD2	EH domain-containing protein 2	0.2	2.08E−10
NP_001104026	FLNA	Filamin-A	0.2	4.46E−29
NP_057371	HP1BP3	Heterochromatin protein 1-binding protein 3	0.3	3.14E−03
NP_001531	HSPB1	Heat shock protein beta-1	0.1	4.17E−09
NP_003861	IQGAP1	Ras GTPase-activating-like protein	0.5	1.54E−03
NP_015556	Kif22	Kinesin family member 22	0.1	1.39E−02
NP_002259	KPNA4	Importin subunit alpha-4	0.3	3.04E−02
NP_059447	MVP	Major vault protein	0.5	1.77E−04
NP_001074419	MYO1C	Myosin-Ic isoform b	0.2	1.84E−05
NP_006087	NDRG1	Protein NDRG1	0.1	4.40E−04
NP_002700	PPP1CB	S/T-protein phosphatase PP1-beta catalytic subunit	0.6	4.19E−02
NP_036364	PTRF	Polymerase I and transcript release factor	0.3	1.06E−06

Table 5 – A list of mitochondrial proteins upregulated in NSCLC cells.

Protein ID	Gene symbol	Description	Fold	*p*-Value
NP_001203	C1QBP	Complement 1 Q subcomponent-binding protein	1.5	3.27E−02
NP_001907	CYC1	Cytochrome c1, heme protein	4.3	3.61E−02
NP_002147	HSPD1	60 kDa heat shock protein	3.3	5.19E−16
NP_573566	LRPPRC	Leucine-rich PPR motif-containing protein	3.9	4.71E−14
NP_006285	UQCRB	Cytochrome b–c1 complex subunit 7	6.1	1.68E−02

are upregulated, although only 5 mitochondrial proteins were detected to be upregulated (with p values <0.05) in cancer cells. This is consistent with our results from another recent study showing that enhanced heme function promotes lung cancer progression [21].

3.4. *Immunofluorescence microscopy confirms that the actin cytoskeletal structure is permanently altered in lung cancer cells*

The iTRAQ results showing the systematic downregulation of many proteins involved in actin cytoskeleton lead us to postulate that actin cytoskeletal structure is dramatically altered in NSCLC cells. To test this idea, we performed immunofluorescence microscopy to compare the formation of actin cytoskeletal structures in the normal HBEC30KT cells and two NSCLC cell lines HCC4017 and A549 (see Fig. 5A and B). We used phalloidin staining to examine and compare stress fiber formation in normal and cancer lung cells. We also stained vinculin in order to examine focal adhesions in the cells [11,22]. Fig. 5 shows the result of microscopic analysis. Clearly, stress fiber formation was very strong and prominent in the normal lung cells, as expected (see the prominent thick red fibers in the HBEC panels of Fig. 5A and B). In the lung cancer cells, however, stress fiber formation was substantially weakened (see the weak and narrow red fibers in the panels HCC and A549). Likewise, stronger and more prominent adhesions were formed in the normal cells, compared to the cancer cells (see the prominent and thick green bands in the panel HBEC in Fig. 5A and B; in panels HCC and A549, only green spots were

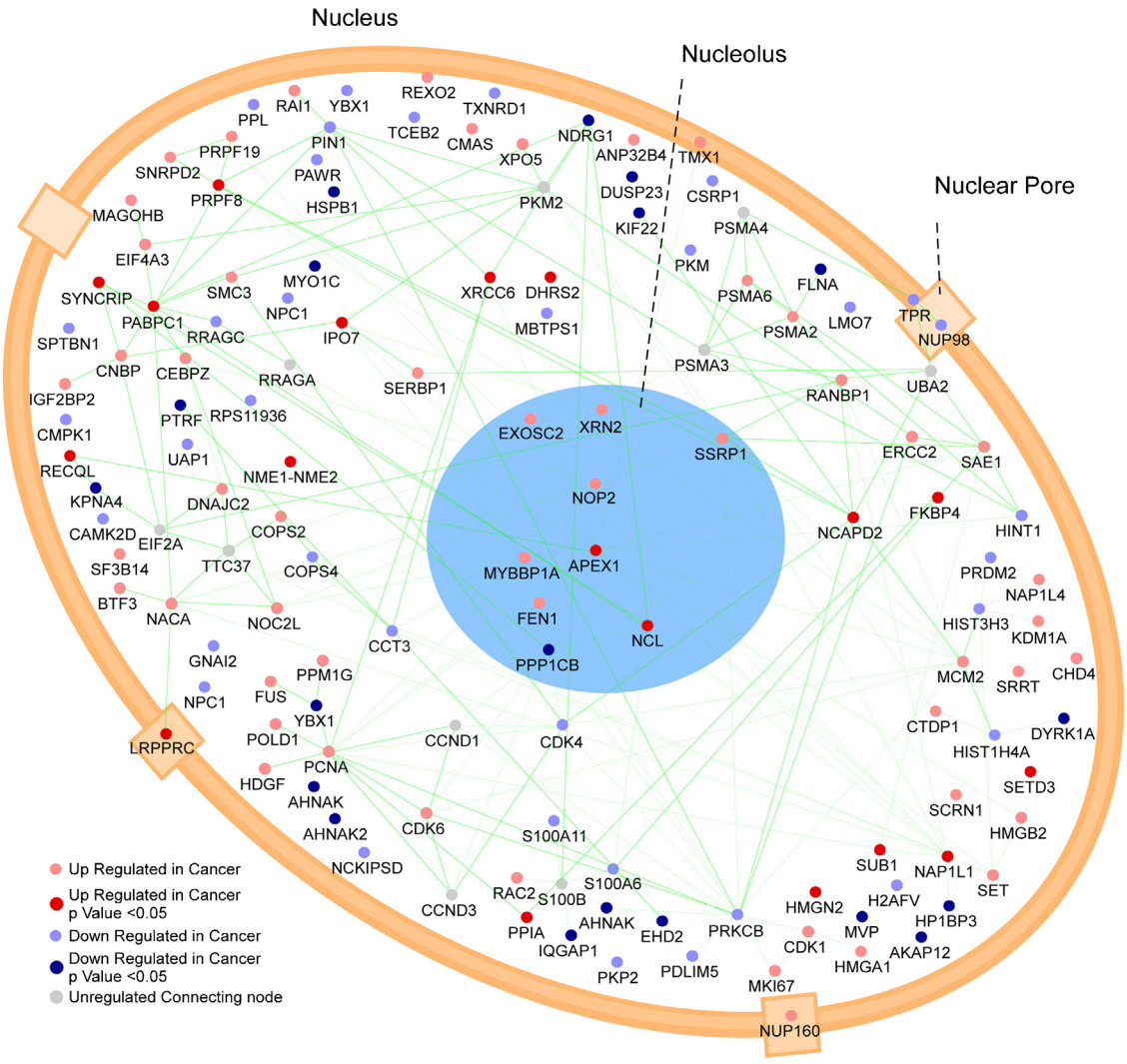

Fig. 3 – Graphical representation of protein–protein interaction networks for up- and downregulated nuclear proteins. The network was constructed in the same manner as Fig. 2. Red and light red nodes represent proteins upregulated in cancer, selected based on both fold changes and *p* values and on fold changes, respectively. Blue and light blue ones represent proteins downregulated in cancer, selected based on both fold changes and *p* values and on fold changes, respectively. Gray nodes represent unchanged proteins present in the network. Lines represent an association of the protein to an interaction, a particular complex or functional GO term. (For interpretation of the references to color in this figure legend, the reader is referred to the web version of the article.)

detected, showing decreased formation of focal adhesions). These results confirmed the results from the iTRAQ studies and showed that the formation of actin cytoskeleton and focal adhesions is permanently altered during the transformation of normal lung cells to NSCLC cells.

4. Discussion

iTRAQ mass spectrometry analysis provides a systematic way to identify the changes in proteins in lung cancer vs. normal cells, in the absence of any preconceived limitation and selection. This approach should identify the most prominent protein changes in cancer cells in an unbiased manner. Using iTRAQ, we detected 1584 proteins in the normal HBEC30KT and cancer HCC4017 lung cells. Among them, the levels of 183 (53 with *p* value cutoff) proteins were significantly upregulated, while the levels of 275 (86 with *p* value cutoff) proteins were downregulated (Table 1). The most striking difference occurred in actin cytoskeleton, where 81 proteins (~3/4 of the detected proteins; 36 with *p* value cutoff) were downregulated, while only 1 was upregulated, among the 118 detected actin cytoskeletal proteins. The main conclusions from using the information from proteins selected by using only fold changes and from using both fold changes and *p* value cutoff are largely the same. Thus, the information gained from the analysis of the larger number of changed proteins may also be biologically relevant. Thus, we included all changed proteins in Figs. 2–4.

The downregulated actin cytoskeletal proteins include mainly those involved in the formation of stress fibers

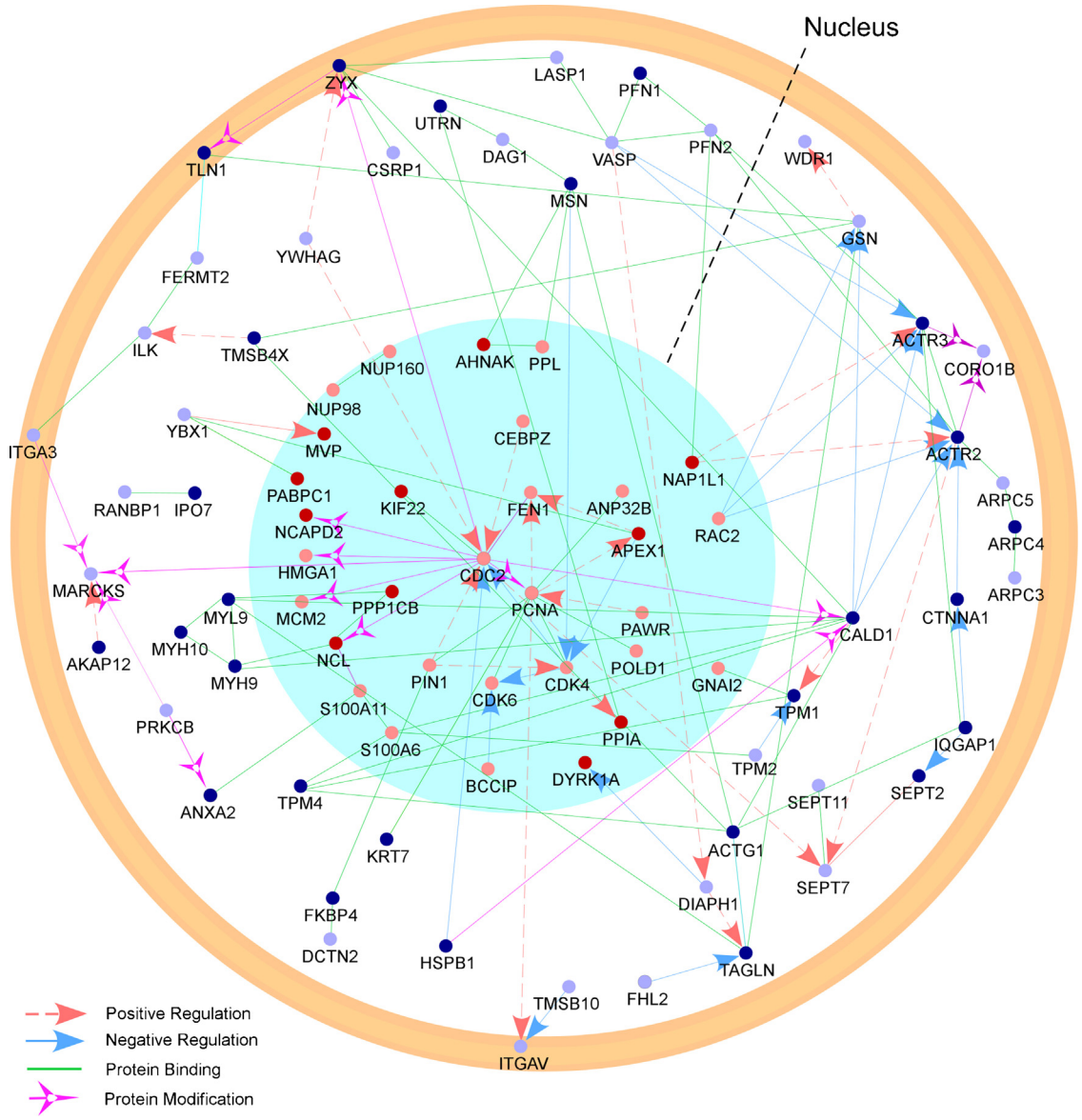

Fig. 4 – Graphical representation of interaction networks for altered nuclear proteins and downregulated actin cytoskeletal proteins. The network was constructed using tools and edge data provided by the Pathway Studios program version 7. Cytoscape was used for network arrangement and CANVAS for final visuals. Red and blue arrows represent positive and negative regulatory edge interaction, respectively. Red and light red nodes represent altered nuclear proteins, selected based on both fold changes and *p* values and on fold changes, respectively. Blue and light blue nodes represent downregulated actin cytoskeletal proteins, selected based on both fold changes and *p* values and on fold changes, respectively. (For interpretation of the references to color in this figure legend, the reader is referred to the web version of the article.)

(both dorsal and ventral), focal adhesions, and cortical actin cytoskeleton (Fig. 2) [16–19]. These proteins include ACTR2 and ACTR3, which are components of the Arp2/3 complex (see Table 2 and Fig. 2). The Arp2/3 complex stimulates the formation of new actin filaments at the leading edge of motile cells, produces branches on the sides of existing filaments, and is important for cell motility [23,24]. Filamin A and B, which are important for regulating the formation of actin cytoskeleton network [25,26], were downregulated. The downregulated proteins also include myosin and tropomyosin chains, inlcuding MYH9, MYH10, MYL6, MYL9, MYO1C, TPM1, TPM3, TPM4 (see Fig. 2 and Table 2), which have important functions in cell motility and its regulation [27,28]. Sept2 and other septins, which are key components of cytoskeleton [29], were downregulated. Many of these proteins are critical for stress fiber formation (Fig. 2) [16,30]. Furthermore, proteins involved in the formation of focal adhesions [17,19,22,31,32], such as PFN1 and TLN1, were downregulated. The downregulation of such a high number of proteins involved in the function and regulation of actin cytoskeleton indicates significant changes in actin cytoskeleton and cell motility in lung cancer cells. Notably, this result is also supported by previous comparative proteomic studies of tumor and normal lung tissues. For example, in the study by Li et al., among only 11 identified proteins that are

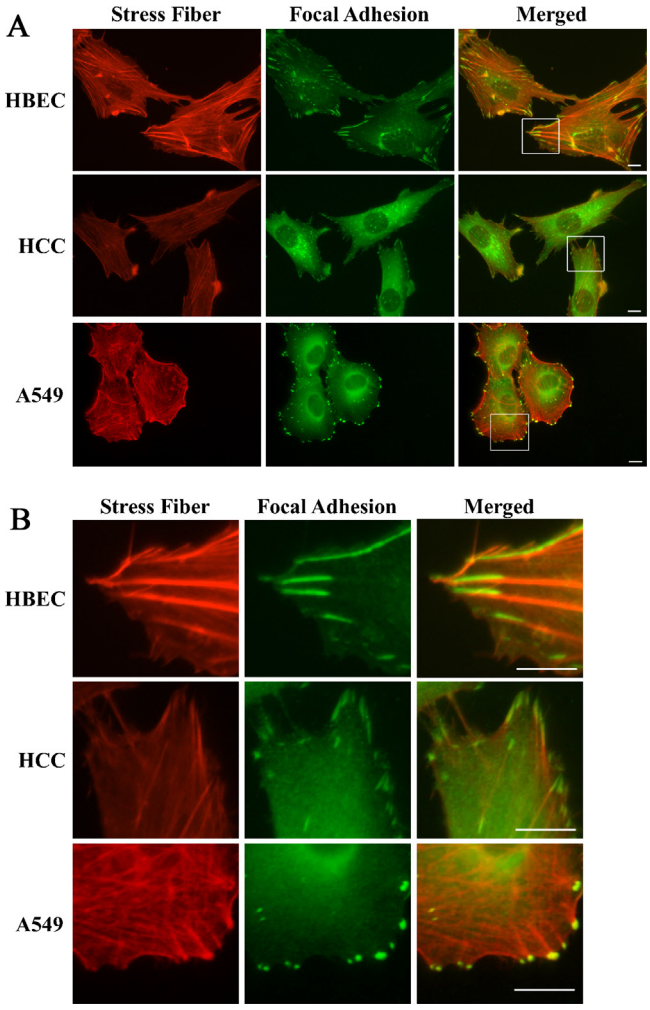

Fig. 5 – Fluorescent microscopic images of stress fibers and focal adhesions formed in normal and cancer lung cells. HBEC30KT, HCC4017 and A549 cells were grown, and F-actin was visualized with Alexa Fluor 568-phalloidin. Focal adhesions were visualized by using a monoclonal anti-vinculin antibody, followed by detection with a FITC-conjugated goat anti-mouse IgG antibody. B shows enlarged version of the boxed areas in A. The bar indicates 10 μm.

decreased in tumor tissues, 3 are actin cytoskeletal proteins [33]. In another study, it was shown that 3 of the 16 downregulated proteins in tumor tissues are actin cytoskeletal proteins [34].

Indeed, the changes in actin cytoskeleton in NSCLC cells were readily confirmed by fluorescent microscopy. Fig. 5 shows that the formation of stress fibers and focal adhesions were substantially diminished in NSCLC HCC4017 and A549 cells, compared to the normal cells. Changes in actin cytoskeleton were found to be critical for malignant tumor formation and for promoting the function of oncogenes in tumor progression more than two decades ago [35]. More recent studies have demonstrated the importance of regulation of actin cytoskeleton in cancer cell migration and invasion. Stabilizing actin cytoskeleton is critical for stopping invading cancer cells and arresting cancer progression [36–39]. Here, our data showed that a systematic and preferential downregulation of actin cytoskeletal proteins diminshes the formation of both stress fibers and focal adhesions, leading to the transformation of normal lung cells to NSCLC cells. While many potential mechanisms can cause changes in actin cytoskeleton [17,18], our data show that the systematic downregulation of many actin cytoskeletal proteins is a key factor in the progression of NSCLC cells. Perhaps this mechanism to change actin cytoskeleton also operates in other kinds of cancer cells.

Additionally, it is worth noting that NAMPT, TAGLN and EphA2, whose changes were confirmed by Western blotting here, have been investigated peviously regarding their roles in lung cancer. NAMPT, nicotinamide phosphoribosyltransferase precursor, is known to be a therapeutic target for lung cancer and inflammation-related disorders [40,41]. Hence, its upregulation in NSCLC cells detected here is consistent with its known role in cancer. A previous study identified NAMPT as one of the genes whose transcript levels are downregulated in lung cancer tissues [42]. There are two reasons that can account for the discrepancy with our results. First, we detected proteins, not mRNA. Second, our data are obtained using homogenous cells, while the previous analyzed data used cancer tissues, which contains a combination of different cell types [42]. Our data showed that the levels of both TAGLN (transgelin) and TAGLN2 proteins were downregulated in NSCLC cells. A previous study has shown that the upregulation of TAGLN expression exerts anti-tumor growth and anti-metastasis effects, whereas its levels are inversely correlated with colorectal cancer metastasis [43]. Another study found that TAGLN is upregulated in the tumor-induced reactive myofibroblastic stromal tissue compartment, while TAGLN2 is upregulated in the neoplastic glandular compartment [44]. These and our results suggest that TAGLN plays an important role in cancer progression.

Further, our Western blotting analysis showed that the levels of both total and ligand-activated (detected by using antibodies to phosphorylated protein) EphA2 proteins were strongly increased in NSCLC cells (Fig. 1C). Eph receptors are shown to play a wide array of roles in cell adhesion and cell movement, as well as in cancer progression [13,15,45–47]. Particularly, the EphA2 receptor has been found to be widely overexpressed in many cancer types [48–50]. The overexpression of EphA2 in NSCLC cells likely contributes to the changes in actin cytoskeleton and adhesions [47].

It is worth noting that a good number of nuclear proteins were up- or downregulated in NSCLC cells (Tables 3 and 4 and Fig. 3). These proteins are involved in diverse functions in the nucleus, and many interact directly with each other (Fig. 3). Interestingly, many of these nuclear proteins also directly interact with the downregulated proteins in actin cytoskeleton (Fig. 4). The changes in the nucleus and actin cytoskeleton may synergize with each other and further promote the transformation of normal cells to cancer cells. This comparative proteomic study of cancer vs. normal cells employing iTRAQ technology and network analysis shows that permanent systematic changes in a large number of cellular proteins accompany the progression of lung cancer cells, and that iTRAQ is a powerful technique to identify such changes.

5. Conclusions

Lung cancer cells exhibit characteristic changes in proteins, when compared to the normal lung epithelial cells. The most dramatic change is the systemic downregulation of many proteins with functions in actin cytoskeleton and adhesion. This downregulation leads to substantial changes in actin cytoskeletal structure, thereby altering cell motility and migration and leading to the progression of lung cancer cells.

Acknowledgments

The HCC4017 and HBEC30KT cell lines were kindly provided by Dr. John Minna's lab. Future requests of the lines should be directed to Dr. Minna. We are grateful to Bruce and Anne Stanley (PennState Hershey College of Medicine) for their effective assistance in iTRAQ mass spectrometry and data analysis. This work was supported by the Cecil H. and Ida Green funds (LZ).

Appendix A. Supplementary data

Supplementary material related to this article can be found, in the online version, at doi:10.1016/j.euprot.2014.01.001.

REFERENCES

[1] Jemal A, Siegel R, Xu J, Ward E. Cancer statistics, 2010. CA Cancer J Clin 2010;60:277–300.
[2] Organization WH. Cancer. Fact sheet no. 297. World Health Organization; 2011.
[3] Ramirez RD, Sheridan S, Girard L, Sato M, Kim Y, Pollack J, et al. Immortalization of human bronchial epithelial cells in the absence of viral oncoproteins. Cancer Res 2004;64:9027–34.
[4] Whitehurst AW, Bodemann BO, Cardenas J, Ferguson D, Girard L, Peyton M, et al. Synthetic lethal screen identification of chemosensitizer loci in cancer cells. Nature 2007;446:815–9.
[5] Ross PL, Huang YN, Marchese JN, Williamson B, Parker K, Hattan S, et al. Multiplexed protein quantitation in *Saccharomyces cerevisiae* using amine-reactive isobaric tagging reagents. Mol Cell Proteomics 2004;3:1154–69.
[6] Aggarwal K, Choe LH, Lee KH. Shotgun proteomics using the iTRAQ isobaric tags. Brief Funct Genomic Proteomic 2006;5:112–20.
[7] Shah AN, Cadinu D, Henke RM, Xin X, Dastidar RG, Zhang L. Deletion of a subgroup of ribosome-related genes minimizes hypoxia-induced changes and confers hypoxia tolerance. Physiol Genomics 2011;43:855–72.
[8] Keshamouni VG, Michailidis G, Grasso CS, Anthwal S, Strahler JR, Walker A, et al. Differential protein expression profiling by iTRAQ-2DLC–MS/MS of lung cancer cells undergoing epithelial–mesenchymal transition reveals a migratory/invasive phenotype. J Proteome Res 2006;5:1143–54.
[9] Tang WH, Shilov IV, Seymour SL. Nonlinear fitting method for determining local false discovery rates from decoy database searches. J Proteome Res 2008;7:3661–7.
[10] Fisher RA. Statistical methods for research workers. 12th ed. Edinburgh: Oliver and Boyd; 1954.
[11] Tojkander S, Gateva G, Schevzov G, Hotulainen P, Naumanen P, Martin C, et al. A molecular pathway for myosin II recruitment to stress fibers. Curr Biol 2011;21:539–50.
[12] Rubporn A, Srisomsap C, Subhasitanont P, Chokchaichamnankit D, Chiablaem K, Svasti J, et al. Comparative proteomic analysis of lung cancer cell line and lung fibroblast cell line. Cancer Genomics Proteomics 2009;6:229–37.
[13] Kandouz M. The Eph/Ephrin family in cancer metastasis: communication at the service of invasion. Cancer Metastasis Rev 2012;31:353–73.
[14] Faoro L, Singleton PA, Cervantes GM, Lennon FE, Choong NW, Kanteti R, et al. EphA2 mutation in lung squamous cell carcinoma promotes increased cell survival, cell invasion, focal adhesions, and mammalian target of rapamycin activation. J Biol Chem 2010;285:18575–85.
[15] Nievergall E, Lackmann M, Janes PW. Eph-dependent cell–cell adhesion and segregation in development and cancer. Cell Mol Life Sci 2012;69:1813–42.
[16] Naumanen P, Lappalainen P, Hotulainen P. Mechanisms of actin stress fibre assembly. J Microsc 2008;231:446–54.
[17] Parsons JT, Horwitz AR, Schwartz MA. Cell adhesion: integrating cytoskeletal dynamics and cellular tension. Nat Rev Mol Cell Biol 2010;11:633–43.
[18] Olson EN, Nordheim A. Linking actin dynamics and gene transcription to drive cellular motile functions. Nat Rev Mol Cell Biol 2010;11:353–65.
[19] Zaidel-Bar R, Itzkovitz S, Ma'ayan A, Iyengar R, Geiger B. Functional atlas of the integrin adhesome. Nat Cell Biol 2007;9:858–67.
[20] Anderson KE, Sassa S, Bishop DF, Desnick RJ. Disorders of heme biosynthesis: X-linked sideroblastic anemia and the porphyrias. In: Scriver CR, Beaudt AL, Sly WS, Valle D, Barton C, Kinzler KW, et al., editors. The metabolic and molecular bases of inherited disease. New York: The McGraw-Hill Companies Inc.; 2009. p. 1–53 [Chapter 124].
[21] Hooda J, Cadinu D, Alam MM, Shah A, Cao TM, Sullivan LA, et al. Enhanced heme function and mitochondrial respiration promote the progression of lung cancer cells. PLoS ONE 2013;8:e63402.
[22] Ziegler WH, Gingras AR, Critchley DR, Emsley J. Integrin connections to the cytoskeleton through talin and vinculin. Biochem Soc Trans 2008;36:235–9.
[23] Pollard TD. Regulation of actin filament assembly by Arp2/3 complex and formins. Annu Rev Biophys Biomol Struct 2007;36:451–77.
[24] Rotty JD, Wu C, Bear JE. New insights into the regulation and cellular functions of the ARP2/3 complex. Nat Rev Mol Cell Biol 2013;14:7–12.
[25] Yue J, Huhn S, Shen Z. Complex roles of filamin-A mediated cytoskeleton network in cancer progression. Cell Biosci 2013;3:7.
[26] Djinovic-Carugo K, Carugo O. Structural portrait of filamin interaction mechanisms. Curr Protein Pept Sci 2010;11:639–50.
[27] Gunning PW, Schevzov G, Kee AJ, Hardeman EC. Tropomyosin isoforms: divining rods for actin cytoskeleton function. Trends Cell Biol 2005;15:333–41.
[28] Hartman MA, Finan D, Sivaramakrishnan S, Spudich JA. Principles of unconventional myosin function and targeting. Annu Rev Cell Dev Biol 2012;27:133–55.
[29] Mostowy S, Cossart P. Septins: the fourth component of the cytoskeleton. Nat Rev Mol Cell Biol 2012;13:183–94.
[30] Pellegrin S, Mellor H. Actin stress fibres. J Cell Sci 2007;120:3491–9.
[31] Campbell ID. Studies of focal adhesion assembly. Biochem Soc Trans 2008;36:263–6.

[32] Zaidel-Bar R, Geiger B. The switchable integrin adhesome. J Cell Sci 2010;123:1385–8.
[33] Li LS, Kim H, Rhee H, Kim SH, Shin DH, Chung KY, et al. Proteomic analysis distinguishes basaloid carcinoma as a distinct subtype of nonsmall cell lung carcinoma. Proteomics 2004;4:3394–400.
[34] Park HJ, Kim BG, Lee SJ, Heo SH, Kim JY, Kwon TH, et al. Proteomic profiling of endothelial cells in human lung cancer. J Proteome Res 2008;7:1138–50.
[35] Holme TC. Cancer cell structure: actin changes in tumour cells—possible mechanisms for malignant tumour formation. Eur J Surg Oncol 1990;16:161–9.
[36] O'Neill GM. Scared stiff: stabilizing the actin cytoskeleton to stop invading cancer cells in their tracks. Bioarchitecture 2011;1:29–31.
[37] Stevenson RP, Veltman D, Machesky LM. actin-bundling proteins in cancer progression at a glance. J Cell Sci 2012;125:1073–9.
[38] Hall A. The cytoskeleton and cancer. Cancer Metastasis Rev 2009;28:5–14.
[39] Yamaguchi H, Condeelis J. Regulation of the actin cytoskeleton in cancer cell migration and invasion. Biochim Biophys Acta 2007;1773:642–52.
[40] Okumura S, Sasaki T, Minami Y, Ohsaki Y. Nicotinamide phosphoribosyltransferase: a potent therapeutic target in non-small cell lung cancer with epidermal growth factor receptor-gene mutation. J Thorac Oncol 2012;7:49–56.
[41] Montecucco F, Cea M, Cagnetta A, Damonte P, Nahimana A, Ballestrero A, et al. Nicotinamide phosphoribosyltransferase as a target in inflammation-related disorders. Curr Top Med Chem 2013;13:2930–8.
[42] Srivastava M, Khurana P, Sugadev R. Lung cancer signature biomarkers: tissue specific semantic similarity based clustering of digital differential display (DDD) data. BMC Res Notes 2012;5:617.
[43] Chunhua L, Donglan L, Xiuqiong F, Lihua Z, Qin F, Yawei L, et al. Apigenin up-regulates transgelin and inhibits invasion and migration of colorectal cancer through decreased phosphorylation of AKT. J Nutr Biochem 2013;24:1766–75.
[44] Rho JH, Roehrl MH, Wang JY. Tissue proteomics reveals differential and compartment-specific expression of the homologs transgelin and transgelin-2 in lung adenocarcinoma and its stroma. J Proteome Res 2009;8:5610–8.
[45] Kaenel P, Mosimann M, Andres AC. The multifaceted roles of Eph/ephrin signaling in breast cancer. Cell Adh Migr 2012;6:138–47.
[46] Pasquale EB. Eph receptors and ephrins in cancer: bidirectional signalling and beyond. Nat Rev Cancer 2010;10:165–80.
[47] Singh A, Winterbottom E, Daar IO. Eph/ephrin signaling in cell–cell and cell–substrate adhesion. Front Biosci 2012;17:473–97.
[48] Ireton RC, Chen J. EphA2 receptor tyrosine kinase as a promising target for cancer therapeutics. Curr Cancer Drug Targets 2005;5:149–57.
[49] Landen CN, Kinch MS, Sood AK. EphA2 as a target for ovarian cancer therapy. Expert Opin Ther Targets 2005;9: 1179–87.
[50] Wykosky J, Debinski W. The EphA2 receptor and ephrinA1 ligand in solid tumors: function and therapeutic targeting. Mol Cancer Res 2008;6:1795–806.